

FY-4A SATELLITE BASED CLOUD MICROPHYSICAL VARIATION ANALYSIS OF AIRBORNE CLOUD SEEDING OPERATIONS IN SICHUAN BASIN

Dan Lin¹, Weijia Wang^{2,*}, Ping Liu¹, Guihua Liu³, Wei Geng⁴

¹ Weather Modification Office of Sichuan Province, CMA, Chengdu, China - ld8768@hotmail.com, sclp1457@163.com

² Chengdu Meteorological Bureau, CMA, Chengdu, China - wjwang1998@163.com

³ Meteorological Institute of Shanxi Province, CMA, Xi'an, China - liu_guihua@163.com

⁴ Sichuan Meteorological Disaster Prevention Technology Center, CMA, Chengdu, China - 63288554@qq.com

Commission III, WG III/8

KEY WORDS: FY-4A, Satellite-Retrieved Microstructure, Precipitation Formation, Cloud Seeding Effect, Effective Radius

ABSTRACT:

Based on a satellite retrieval methodology, the cloud microphysical properties of two airborne cloud seeding operations in Sichuan Basin of Southwest China are analyzed in this paper. The methodology for the retrieval of the cloud particle effective radius (R_e), cloud temperature (T) and microphysical structure is based on the data from the AGRI onboard the Chinese FY-4A satellite. A microphysical red–green–blue (RGB) composite visualization has been devised to qualitatively highlight the cloud composition. This RGB scheme is displayed by compositing visible 0.65 micron channel, near infrared 2.2 micron channel and infrared 11.0 micron channel. And the vertical structure and development status of the clouds are demonstrated by the T - R_e profiles. The results show that after the cloud seeding operation on June 11, 2018, the cloud particle effective radius increases, and the ground observed PM_{10} and $PM_{2.5}$ pollutants decrease as well. As for the cloud seeding operation on November, 17, 2018, the satellite inversion shows that the medium and low level clouds are rich in super-cooled water with small cloud particle effective radius. After the cloud seeding operation, the effective radius of the cloud droplets increases significantly. Both of these two cloud seeding operation in Sichuan Basin demonstrate obvious precipitation enhancement results in the seeding impact area.

1. INTRODUCTION

With the rapid development of meteorological satellites, multi-spectral data with high spatial and temporal resolution can be obtained. Therefore, the meteorological satellites can provide information on the development and evolution of clouds and precipitation, making up for the shortage of ground-based observations. Meanwhile, the satellite data can help to better understand cloud microphysical structure and precipitation formation and provide new ideas for cloud-precipitation interaction research (Sheng et al., 2010). At home and abroad, some research has been done on satellite remote sensing inversion of cloud characteristics (Liu et al., 2003; Arking and Childs, 1987; Pavolonis et al., 2005), and many applications of satellite data and inversion products in artificial weather modification have been carried out. Meteorological satellites can detect the macro and micro characteristics of clouds, and obtain cloud parameters such as cloud water content and particle effective radius. By using CLOUDSAT and CALIPSO satellite data, Ding et al. (Ding et al., 2012) analyzed the macro and micro vertical structure characteristics of different cloud types in Northwest China. It is found that the probability density distribution in the vertical direction of clouds has significant regional and seasonal characteristics, and there are abundant cloud water resources in the lower layer in summer. Rosenfeld et al. (Rosenfeld et al., 2005) found that NOAA AVHRR images could reveal conspicuous tracks of glaciated clouds in thick super-cooled layer clouds over central China. And these tracks were identified as being artificially produced by cloud seeding operations by means of silver iodide acetone generators. Based on RGB composite images from the NOAA-

18 polar orbit satellite data and the FY-2C geostationary orbit satellite data, Liu et al. (Liu et al., 2011a) analyzed a topographic cloud seeding in Northern Shanxi and found that the low clouds whose temperature are about $-20\text{ }^{\circ}\text{C}$ produce more precipitation due to the involvement of high clouds above them in the rain process. A 3-minute 3-km rapid scan of the METEOSAT Second Generation geostationary satellite over Southern Africa was applied to track the evolution of cloud top temperature (T) and particle effective radius (R_e) of convective elements by Lensky and Rosenfeld (Lensky and Rosenfeld, 2006). And it is found that the evolution of T - r_e relations shows little dependence on time, leaving particle effective radius to depend almost exclusively on temperature. Based on these findings, the cloud microphysical structure and the precipitation formation process during and after two cloud seeding operations are analyzed in this paper based on the satellite retrieval methodology developed by Rosenfeld and Liu and the latest Chinese meteorological satellite data.

The higher resolution data from the FY-4A can supply more information and depict more detailed microphysical structure of cloud and precipitation than the previous lower resolution data. Thus, the purpose of this paper is to highlight the microphysical retrievals obtained from the FY-4A data and their application in the understanding of microphysical properties and the cloud and precipitation formation processes during two airborne cloud seeding operations.

* Corresponding author: Weijia Wang

2. DATA

2.1 Satellite Data

The Advanced Geosynchronous Radiation Imager (AGRI) mounted onboard the FY-4A, the latest Chinese FengYun (FY) geostationary orbit meteorological satellite, installs 14 spectral bands with a spectral coverage from 0.47 micron (visible band) to 13.5 micron (infrared band) and a full-disk observation frequency of 15 min (Zhang et al., 2019). Compared with the FY-2 satellites, the FY-4A satellite further strengthens the ability to monitor clouds by providing continuous measurements on optical thickness, liquid water content, phase state, cloud top pressure. In this paper, the FY-4A satellite data are mainly used to conduct inversion of various physical parameters of cloud precipitation in Sichuan Basin. The variation characteristics of physical parameters of clouds during two airborne cloud seeding operations on June 11, 2018 and November 17, 2018 are analyzed. The AGRI in the FY-4 satellite has the advantages of large range, high time and space resolution. Multi-channel synthesis technology can be used to generate cloud micro-physical images and cloud phase images, which can effectively identify and track super-cooled water areas, and obtain cloud microscopic characteristics and evolution of clouds. In 2005, Shanxi Meteorological Research Institute introduced satellite inversion technology that was established by Rosenfeld, developed cloud micro-physical inversion technology methods based on NPP, MODIS and FY data, and then applied them to the analysis of cloud precipitation and artificial precipitation enhancement operation (Dai et al., 2006; Dai et al., 2011). The satellite inversion products used in this paper are generated based on this technology.

2.2 RGB Composite Images

Based on the high spatial resolution of the AGRI onboard the FY-4A (from 0.5 km in the visible band to 4.0 km in the infrared band), a microphysical red–green–blue composite visualization has been devised to qualitatively highlight the cloud composition. Microphysical RGB composite imagery is displayed by compositing visible 0.65 micron channel, near infrared 2.2 micron channel and infrared 11.0 micron channel. The red (R), green (G) and blue (B) color values are assigned to these three channels. Through combination coding, RGB images are formed (Liu et al., 2009).

As for the retrieval of the FY-4A satellite data, the cloud temperature (T) is given by the 11.0 micron brightness temperature, and the effective radius of the cloud droplets (R_e) is approximated by the 2.2 micron reflectance component. The red is modulated by the visible reflectance. 11.0 micron channel brightness temperature depends on the cloud height, the higher the cloud is, the lower the brightness temperature is, and the lower the blue tone is. 2.2 micron channel reflectance depends on the size of the cloud droplets, the smaller the cloud droplet is, the larger the reflectance is, and the higher the green tone is. The visible 0.65 micron channel reflectance depends on the cloud optical thickness. The higher the cloud optical thickness is, the higher the visible light reflectance is, and the higher the red tone is. The RGB images can be used to invert the characteristics of different types of clouds and surface, identify different types of clouds, and analyze more information about the formation process of cloud precipitation from the different cloud thickness, particle size and cloud top height.

2.3 T-Re Profiles

Most meteorological satellite observation can only obtain the information on the top of clouds. If there are clouds of different heights in a certain area, the atmospheric temperature, dew point and cloud condensation nucleus (CCN) conditions in this region are similar, then the air rises, cools and saturate condenses to form these clouds, and these clouds will have similar cloud base height, number concentration of cloud droplets and particle size. If the water content of cloud droplets increases at the same height, the cloud particles grow in similar sizes. Therefore, it can be assumed that the effective radius near the cloud top is similar to the effective radius in the cloud at the same height. This assumption of the retrieval method is that time and space are exchangeable, so the composition of the tops of various clouds reaching different heights in a convective cluster at a given time is similar to the time evolution of a cloud-top composition as it grows up with time (Lensky and Rosenfeld, 2006).

By selecting clouds of different heights, the change curve of cloud particle effective radius (R_e) with temperature (T) can be obtained. Firstly, select the analysis region, and count the R_e in this region at 1 °C intervals. Then arrange all R_e at the same temperature in the region from smallest to largest. Since the number of R_e at the same temperature is different, normalization process is carried out. The percentage of sample number is determined with 5% as the interval, 5% as the R_e of the 5% sample, and 20% as the R_e of the 20% sample. Finally, select 10%, 25%, 50%, 75%, 90% sample percentages and draw T- R_e (Dai et al., 2010).

3. RESULTS

3.1 Airborne Cloud Seeding Operation on June 11, 2018

3.1.1 Cloud Seeding Process : An airborne precipitation enhancement operation was conducted from 15:10 LST to 18:10 LST, June 11, 2018, in Southern Sichuan Basin, with 20 silver iodide flares used as seeding material. The aircraft began seeding at 15:40 LST and finished seeding at 17:00 LST. The cloud seeding route was designed like the letter ‘S’ and the real seeding flight path is shown in Figure 1. According to the airborne observation records, the seeding altitude is between 5300 m and 5600 m, the temperature of seeding layer is between -6 °C and -9 °C, the wind speed of the seeding layer is about 12m/s, and the wind direction is southwest.

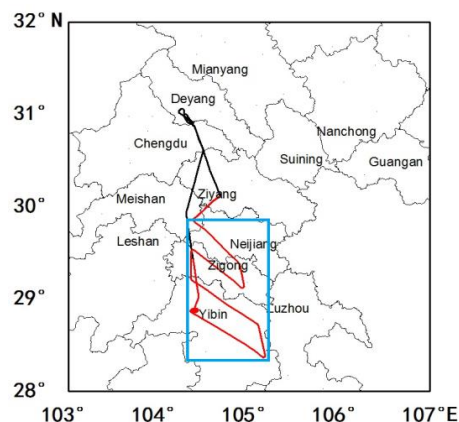


Figure 1. Cloud seeding flight path on June 11, 2018 (flight path in black line, seeding path in red line, seeding impact area in azure box)

3.1.2 Cloud Seeding Effect: Figure 2 and figure 3 are the FY-4A inversion RGB image and T-Re profiles at 16:38 LST respectively. It can be seen from the figure that the color of cloud in the seeding region is mainly pink and yellow. The cloud top temperature is between -7°C and -21°C , and the effective radius of the cloud droplets is between 12 micron and 29 micron. There are both high and low clouds in this region. In the low clouds, there are many yellow clouds which are rich in super-cooled water. The high clouds that develop on the low clouds are red with larger particle effective radius and lower cloud top temperature. According to the rainfall data from ground meteorological stations, precipitation has been detected in Zigong and Yibin city.

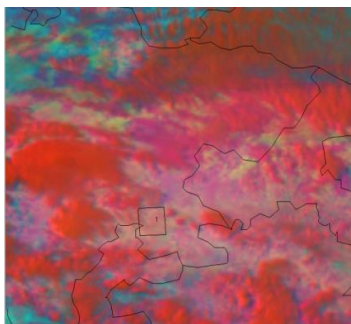


Figure 2. RGB image at 16:38 LST

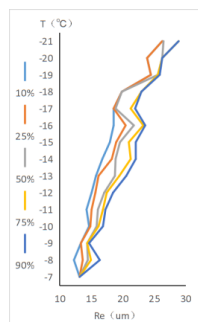


Figure 3. T-Re profiles at 16:38 LST

Considering the diffusion of the seeding material, the wind speed and direction in the seeding cloud layer are used to calculate the spatial distribution region of the seeding material, i.e. the cloud seeding impact area. Figure 4 and figure 5 are the FY-4A inversion RGB images and T-Re profiles after operation at 17:38 LST and 17:53 LST respectively. At 17:38 LST, the clouds in the impact area become darker, and there are mainly red and yellow clouds. According to the principle of RGB image, the cloud develops deeper. The cloud particle size increases from 12 micron to 40 micron, and the cloud top temperature decreases from -11°C to -26°C . At 17:53 LST, in the impact area, the range of red cloud area becomes wider and the cloud continues to develop. The particle effective radius is 11 micron to 40 micron, and the cloud top temperature is -11°C to -25°C . Compared with the cloud parameters during operation, it is found that with the development of the cloud after the operation, the effective radius increases significantly and the cloud top temperature decreases significantly.

The micro-physical processes in the cloud can be divided into condensation growth process, collision growth process, rain embryo formation process, mixed phase growth process and ice growth process. These five processes in the same cloud may not

exist at the same time. When the temperature is lower than 0°C , ice and liquid are both exist, and the effective radius increases rapidly with the height. After growing to 33 micron, the cloud particles are in ice phase. At 16:38 LST, the effective radius of the cloud droplets at -15°C layer is between 17 micron and 22 micron, and the particle effective radius at -20°C layer is about 25 micron. After operation at 17:38 LST, the effective radius of the cloud droplets at -15°C layer is between 15 micron and 27 micron, and the effective radius of the cloud droplets at -20°C layer is between 20 micron and 35 micron. At 17:53 LST, the effective radius of the cloud droplets at -15°C layer is between 15 micron and 35 micron, and the effective radius of the cloud droplets at -20°C layer is between 25 micron and 40 micron. By analyzing the particle effective radius at different heights, it can be seen that before the operation at 16:38 LST, the -15°C and -20°C layers are in the process of collision growth and mixing growth, and both ice and liquid are existing. After operation at 17:53 LST, the average effective radius of the cloud droplets at -20°C layer reaches 33 micron. The cloud droplets are almost completely iced, which has entered the ice growth process, and could provide a large number of solid particles. The -15°C layer is rich in super-cooled water, which is good for the growth of falling solid particles. At 18:00 LST after operation, the average rainfall in the impact area exceeds 1 mm, and the rainfall in some stations exceeds 1.5 mm.

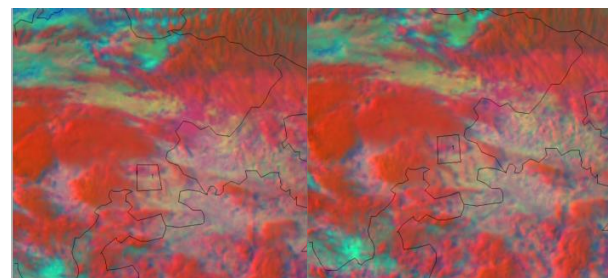


Figure 4. RGB image (left:17:38 LST, right:17:53 LST)

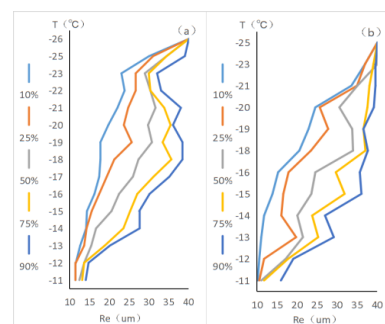


Figure 5. T-Re profiles (left:17:38 LST, right:17:53 LST)

Aerosol concentration is related to meteorological conditions, such as wind speed and precipitation, etc. Precipitation can clear aerosol particles (Zhou et al., 2015). The change of air quality is a continuous and slow process. AQI, PM_{10} and $\text{PM}_{2.5}$ concentrations are calculated at two stations in Yibin city from 15:00 to 20:00 LST (Figure. 6). As can be seen from the figure, the air quality index and the concentration of aerosol particles show a continuous decreasing trend. The change is more obvious at 17:00, AQI reduces significantly. Compared with $\text{PM}_{2.5}$, PM_{10} decreases more greatly, from $100 \mu\text{g}/\text{m}^3$ and $50 \mu\text{g}/\text{m}^3$ at 15:00 LST to $65 \mu\text{g}/\text{m}^3$ and $45 \mu\text{g}/\text{m}^3$ at 17:00 LST. And then AQI, PM_{10} and $\text{PM}_{2.5}$ keep going down, at 20:00 LST, AQI drops to nearly 45, PM_{10} and $\text{PM}_{2.5}$ drop to about $45 \mu\text{g}/\text{m}^3$

and $25 \mu\text{g}/\text{m}^3$ respectively. In general, the concentration of pollutants decreases and the air quality index reaches an excellent level after the seeding operation.

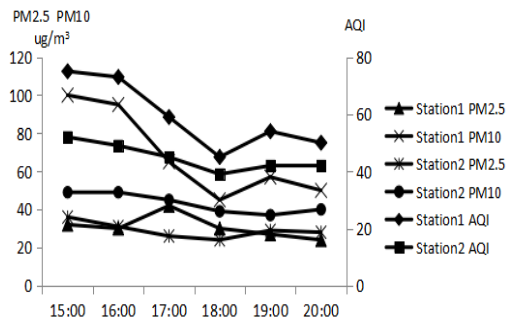


Figure 6. Time variation of AQI, PM_{10} and $\text{PM}_{2.5}$

3.2 Airborne Cloud Seeding Operation on Nov. 17, 2018

3.2.1 Cloud Seeding Process: On November 17, 2018, the cloud seeding aircraft took off from Guanghan airport at 11:40 LST, arrived at Nanchong city and began cloud seeding at 12:00 LST. The seeding was carried out along the "S" route. The seeding lasted 60 min and ended at 13:00 LST. The seeding path is shown in figure 7. According to the airborne observation records, the seeding altitude is about 5000 m, the temperature of the seeding layer is about $-8 \text{ }^\circ\text{C}$, the wind speed is about 15m/s, and the wind direction is westerly, which is similar to the sounding data of Dazhou station ($107.3 \text{ }^\circ\text{E}$, $31.12 \text{ }^\circ\text{N}$) at 08:00 LST.

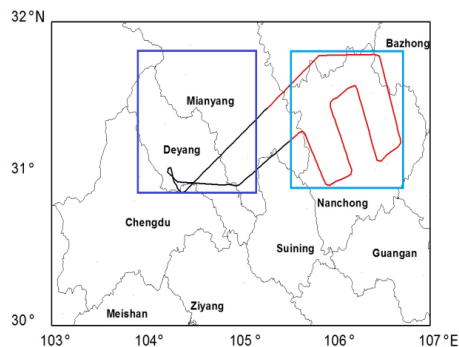


Figure 7. Cloud seeding flight path on November 17, 2018 (flight path in black line, seeding path in red line, impact area in azure box, contrast area in blue box)

3.2.2 Cloud Seeding Effect: Figure 8 and figure 9 are RGB image and T-Re profiles respectively at 11:30 LST. Most areas of Sichuan Basin are covered by clouds mainly in yellow, light red, purple and green color. Region 3 is yellow, light red and green cloud area. The cloud top temperature is higher between $0 \text{ }^\circ\text{C}$ and $-7 \text{ }^\circ\text{C}$, and the particle effective radius is smaller, less than 10 micron, indicating that this area is covered by low clouds with mainly liquid particles. Region 1 is a purple-red cloud area. In this region, cloud top temperature ranges from $-10 \text{ }^\circ\text{C}$ to $-19 \text{ }^\circ\text{C}$, the particle effective radius ranges from 15 micron to 35 micron and up to 40 micron. Thus, this region is a cold cloud region with larger cloud droplets or sufficient ice crystals, which can effectively start the process of collision, growth and ice transformation. Rainfall has been detected by ground automatic stations in region 1. The average hourly rainfall exceeds 1 mm, indicating that there is a good correspondence between region 1 and rainfall. Region 2 is yellow and light-red cloud area. The cloud top temperature is

between $-9 \text{ }^\circ\text{C}$ and $-13 \text{ }^\circ\text{C}$, and the effective radius of the cloud droplets is between 7 micron and 12 micron. Compared with region 1, cloud droplets are relatively small in region 2. According to the method for determining particle phase by using effective radius and temperature of cloud particles proposed by Dai et al. (Dai et al., 2010), when the particle effective radius is less than 15 micron and the cloud top temperature is lower than $0 \text{ }^\circ\text{C}$, the particles mainly exist as liquid droplets. Therefore, region 2 mainly contains abundant super-cooled water. Liu et al. (Liu et al., 2011b) have found that without high clouds, precipitation is small and cloud particles mainly grow up through the condensation process. When the particle effective radius increases to 14 micron or more, some large drops could reach the ground. In the case of high clouds, high clouds can provide a large number of ice crystals for low clouds, and low clouds contain abundant super-cooled water, which could lead to large precipitation. Region 1 is in the case of high cloud, but there is no high cloud in region 2. Only low and medium clouds in region 2 just generate less precipitation. Thus, at this time, region 2 is suitable for seeding operation with cold cloud catalyst, so as to start the transformation process between liquid to ice.

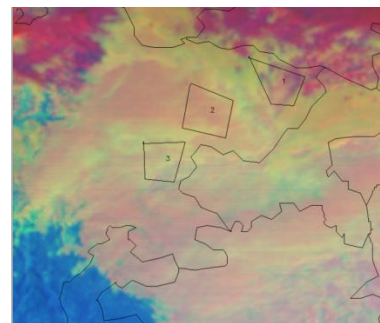


Figure 8. RGB image at 11:30 LST

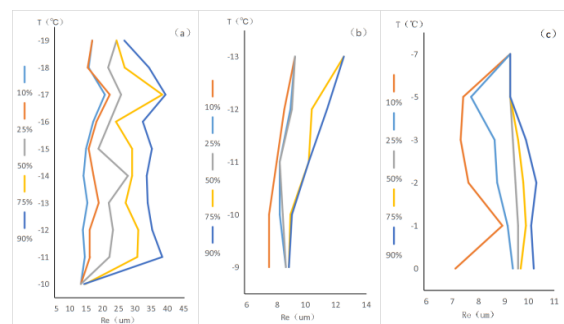


Figure 9. T-Re profiles at 11:30 LST (a: region 1; b: region 2; c: region 3)

Figure 10 and figure 11 are respectively the RGB image and T-Re profiles at 12:30 LST. At this time, the seeding operation is under way. As can be seen from the figure, the seeding region is mainly pink and yellow cloud. Considering the wind speed and direction, this cloud area is thought to have moved here from the yellow and light red cloud area at 11:30 LST. The cloud top temperature in the seeding region is between $-9 \text{ }^\circ\text{C}$ and $-12 \text{ }^\circ\text{C}$, and the effective radius of the cloud droplets is between 8 micron and 11 micron. Compared with 11:30 LST, cloud characteristic parameters do not change significantly, the cloud system develops slowly. The particle effective radius is still small without large drop or ice crystal in the cloud. Historical studies have shown that cloud droplets at this stage mainly grow and become larger through condensation. When they grow to 15 micron, they will fall to the ground due to the inability of

updraft to lift large droplets. In this way, only a small amount of precipitation can be generated.

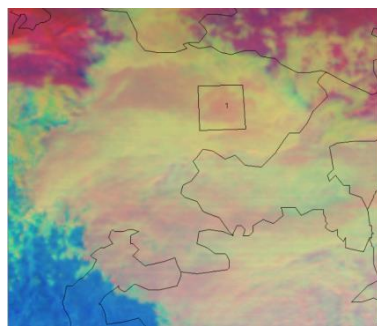


Figure 10. RGB image at 12:30 LST

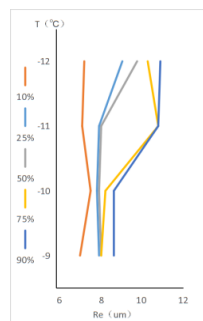


Figure 11. T-Re profiles at 12:30 LST

Considering the similar climate and the same size with the impact area, the contrast area is chosen on the upwind side (Figure 7). And there are an appropriate isolation belt between the contrast area and the impact area. According to the RGB image, the cloud conditions in the two regions are similar. According to the cloud moving speed of 15m/s, it is estimated that the cloud is moving about 0.5° per hour to the east. Then, move position of the impact area and contrast area.

RGB images of 14:30, 14:53 and 15:53 LST are selected as the physical quantity change images after seeding operation for 2 hours and 3 hours. At 14:30 LST (Figure 12-13), region 1 is the impact area, and region 2 is the contrast area after moving. The cloud top temperature in region 1 ranges from -7°C to -20°C , and the particle effective radius ranges from 8 micron to 21 micron. Dai et al. (Dai et al., 2010) have pointed out that when the particle effective radius is greater than 33 micron, most particles are ice phase; when the particle effective radius is less than 15 micron, most particles are liquid phase; when the particle effective radius is between 15 micron and 33 micron, there are both ice and liquid phase particles. Rosenfeld and Gutman (Rosenfeld and Gutman, 1994) have proposed that if the particle effective radius is greater than 14 micron, precipitation could be generated in the cloud. Thus, it indicates that there are particles in ice and liquid phase in region 1, and precipitation particles have started to form in the cloud. After operation, the cloud top temperature decreases significantly, the cloud top height increases and the cloud developments. This cloud conditions are conducive to the growth of cloud particles, so the particle effective radius increases significantly, which could promote the transformation process of liquid to ice, and lead to the growth of large droplets and ice particles in the cloud. Most clouds in region 2 are yellow clouds. The particle effective radius ranges from 7 micron to 13 micron, and the cloud top temperature ranges from -7°C to -12°C . The cloud

conditions in region 2 are similar to those in the operation area at 12:30 LST, indicating that cloud without seeding catalyst develops slowly. At 14:53 LST (Figure 14-15), the particle effective radius in region 1 decreases to 6 micron to 15 micron, the cloud top temperature rises to -7°C to -15°C , and the cloud development in the impact area weakens. Region 2 is still yellow and pink cloud area. The particle effective radius is between 6 micron and 10 micron, and the cloud top temperature is between -7°C and -11°C , indicating that the cloud process without seeding catalyst is still developing slowly. At 15:53 LST (Figure 16-17), the color of cloud in region 1 darkens, changing to green, pink and yellow. The particle effective radius decreases to 5 micron to 13 micron, and the cloud top temperature rises to -7°C to -13°C . In region 2, the particle effective radius is about 5 micron to 14 micron, the cloud top temperature drops slightly from -8°C to -13°C . In general, 2 hours after seeding operation (nearly at 14:30 LST) is the best time for operation influence. The particle effective radius increases significantly in the impact area, the cloud top temperature decreases, and then the cloud development weakens with decreasing particle effective radius and increasing the cloud top temperature. The clouds in contrast area develop slowly from 12:30 to 15:53 LST with no obvious change trend.

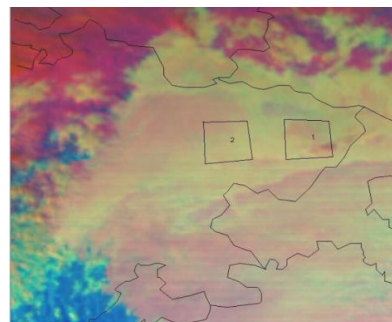


Figure 12. RGB image at 14:30 LST

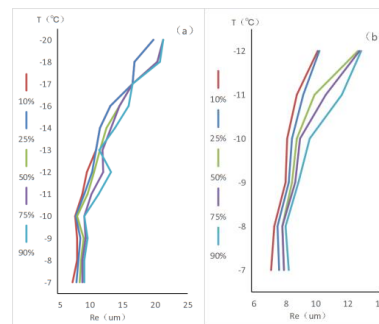


Figure 13. T-Re profiles at 14:30 LST
 (a: region 1; b: region 2)

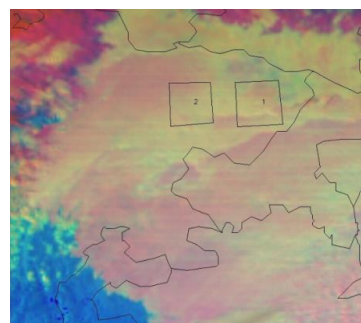


Figure 14. RGB image at 14:53 LST

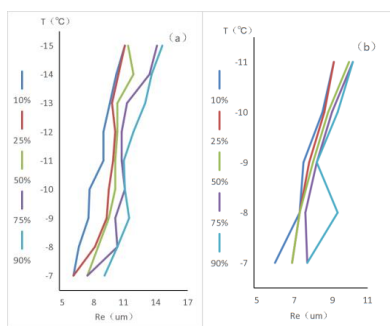


Figure 15. T-Re profiles at 14:53 LST
 (a: region 1; b: region2)

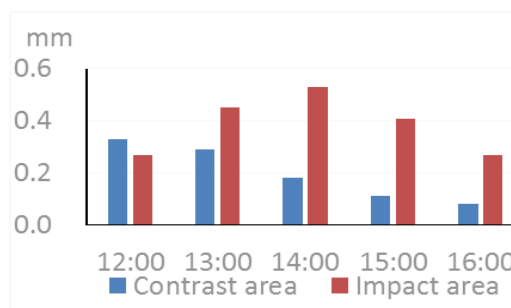


Figure 18. Ground rainfall variation

4. CONCLUSIONS

An airborne cloud seeding operation is carried out in Southern Sichuan Basin on June 11, 2018. After the cloud seeding operation, the effective radius of the cloud droplets increases significantly and the cloud top temperature decreases significantly. The average effective radius of the cloud droplets in the -20 °C layer reaches 33 micron, providing a large number of ice particles. The -15 °C layer is rich in super-cooled water, which could be conducive to the growth of ice particles when they fall down. The rainfall amounts from the ground meteorological stations continue to increase after the cloud seeding operation. Moreover, the concentration of PM₁₀ and PM_{2.5} pollutants decrease and the air quality index reaches an excellent level after the seeding operation.

An airborne cloud seeding operation is carried out in Northern Sichuan Basin on November 17, 2018. After the cloud seeding operation, the cloud particle effective radius in the impact area increases significantly, the cloud top temperature decreases significantly and the clouds continue to develop, which could promote the transformation process from liquid to ice, and lead to the growth of large droplets and ice particles in the clouds. The clouds in the contrast area develop slowly with no obvious change. The rainfall amounts from the ground meteorological stations in the cloud seeding impact area are obviously greater than those in the contrast area.

Based on the FY-4A satellite retrieval RGB images and T-Re profiles, both of these two cloud seeding operation in Sichuan Basin of Southwest China demonstrate obvious precipitation enhancement results in the seeding impact area.

ACKNOWLEDGEMENTS

This work is supported by Sichuan Science and Technology Program 2019YJ0621, Chengdu Science and Technology Program 2018-ZM01-00038-SN, Science and Technology Activity Funding Project for Overseas Returnees 2018-72.

REFERENCES

- Arking, A., Childs, J. D., 1985. Retrieval of cloud cover parameters from multispectral satellite images. *J. Climate Appl. Meteor.*, 24, 322-333.
- Dai, J., Yu, X., Rosenfeld, D., et al., 2006. Analysis of satellite observed microphysical signatures of cloud seeding tracks in supercooled layer clouds. *Acta Meteorologica Sinica*, 66(5), 22-630.

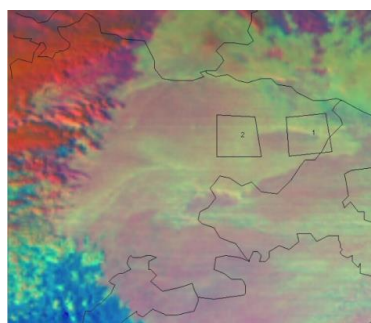


Figure 16. RGB image at 15:53 LST

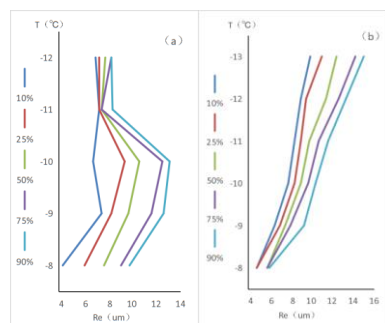


Figure 17. T-Re profiles at 15:53 LST
 (a: region 1; b: region 2)

According to the movement of clouds, the average rainfall in the impact area and the contrast area from 12:00 to 16:00 LST are calculated respectively (Figure 18). At 12:00 LST before the operation, the rainfall is about 0.3 mm in the impact area. The rainfall in the impact area begins to increase and exceeds 0.5 mm during seeding operation. After operation, the rainfall in the impact area remains at about 0.55 mm at 14:00 LST and then decreases to 0.3 mm at 15:00 LST. The rainfall in the contrast area basically maintains between 0.3 mm and 0.4 mm with a small fluctuation during 12:00 to 16:00 LST. Combined with satellite data, the particle effective radius in the impact area increases and the cloud top temperature decreases significantly at 14:30 LST. The particle effective radius starts to decrease from 14:53 LST, and then continues to decrease with increasing cloud top temperature. The changes in physical quantities of cloud characteristics are well matched with ground rainfall. At 14:00 LST, it is the peak period of ground rainfall. At 15:00 LST, it starts to decrease. At 16:00 LST, the rainfall is smallest. The physical quantities of cloud characteristics in the contrast area change little between 14:30 and 15:53 LST. The clouds develop slowly, and there is also no obvious change in ground rainfall.

Dai, J., Yu, X., Liu, G., et al., 2011. Satellite retrieval analysis on micro-physical property of thunderstorm with light precipitation over the Qinghai-Xizang plateau. *Plateau Meteorology*, 30(2), 288-298.

Dai, J., Yu, X., Liu, G., et al., 2010. Analyses of satellite retrieval microphysical properties of a rainstorm in the northern part of Shaanxi. *Acta Meteorologica Sinica*, 68(3), 387-397.

Ding, X., Huang, J., Li, J., et al., 2012. Study on cloud vertical structure feature over Northwest China based on active satellite remote sensing and its influence on precipitation enhancement. *J. Arid Meteor.*, 30(4), 529-538.

Lensky, I., Rosenfeld, D., 2006. The time-space exchangeability of satellite retrieved relations between cloud top temperature and particle effective radius. *Atmospheric Chemistry and Physics*, 6, 2887-2894.

Liu, J., Dong, C., Zhang, W., 2003. Determination of the optical thickness and effective radius of water clouds by FY-1C data. *Journal of Infrared and Millimeter Waves*, 22, 436-440.

Liu, G., Yu, X., Dai, J., 2009. Satellite retrieval of microphysical properties for different cumuli. *Journal of Nanjing Institute of Meteorology*, 32(1), 17-23.

Liu, G., Yu, X., Dai, J., et al., 2011a. A case study of the conditions for topographic cloud seeding based on the retrieval of satellite measurements. *Acta Meteorologica Sinica*, 69(2), 363-369.

Liu, G., Yu, X., Jia, L., et al., 2011b. Satellite observation on rainfall enhancement in stratiform clouds over Shaanxi Province in Spring 2009. *Arid Zone Research*, 2(4), 699-704.

Pavolonis, M. J., Heidinger, A. K., Uttal, T., 2005. Daytime global cloud typing from AVHRR and VIIRS: Algorithm description, validation and comparisons. *J. Appl. Meteor.*, 44, 804-826.

Rosenfeld, D., Gutman, G., 1994. Retrieving microphysical properties near the tops of potential rain clouds by multispectral analysis of AVHRR data. *Atmospheric Research*, 34, 259-283.

Rosenfeld, D., Yu, X., Dai, J., 2005. Satellite-retrieved microstructure of AgI seeding tracks in supercooled layer clouds. *J. Appl. Meteor.*, 44, 760-767.

Sheng, R., Gong, T., Wang, Q., et al., 2010. Correlation analysis of satellite retrieved cloud characteristics and surface precipitation. *Meteorological Science and Technology*, 38(S), 68-73.

Zhang, P., Lu, Q., Hu, X., et al., 2019. Latest progress of the Chinese meteorological satellite program and core data processing technologies, *Advances In Atmospheric Sciences*, 36(9), 1027-1045.

Zhou, B., Liu, R., Wei, J., et al., 2015. A preliminary analysis on scavenging effect of precipitation on aerosol particles. *Resources and Environment in the Yangtze Basin*, S1, 160-170.